International Journal of Heat and Fluid Flow 30 (2009) 140–149

Contents lists available at ScienceDirect

International Journal of Heat and Fluid Flow

journal homepage: www.elsevier.com/locate/ijhff

Experimental investigation of micro-scale temperature transients in sub-cooled flow boiling on a horizontal heater

M. Sunder, D. Banerjee *

Department of Mechanical Engineering, Texas A&M University, College Station, TX 77843, United States

ARTICLE INFO

Article history:
Received 13 February 2008
Received in revised form 31 July 2008
Accepted 6 August 2008
Available online 28 November 2008

Keywords:
Flow boiling
Thin film thermocouple
Microfabrication
Nanofabrication
Fast Fourier transform

ABSTRACT

Surface temperature fluctuations that occur locally underneath departing bubbles in pool boiling are shown to result in local heat transfer coefficients ranging from 1 to 10 kW/cm^2. These estimates were reported in the literature involved both numerical and experimental approaches. Significantly higher heat fluxes are associated with flow boiling than pool boiling under similar conditions of wall superheat and liquid subcooling (e.g. at boiling inception and at critical heat flux). These enhancements are primarily caused by the convective transport, acceleration/distortion of the bubble departure process as well as the resultant potential enhancement of the local surface temperature fluctuations.

In this study we measure the surface temperature fluctuations using temperature micro/nano-sensors fabricated on a silicon wafer during flow boiling on the silicon wafer which is heated from below. The silicon wafer is clamped on a constant heat flux type calorimeter consisting of a vertical copper cylinder with embedded cartridge heaters and K-type thermocouples. Micro/nano-thermocouples (thin film thermocouples or "TFT") are fabricated on the surface of the silicon wafer. High speed data acquisition apparatus is used to record temperature data from the TFT at 1 kHz. A fluorinert was used as the test fluid (PF-5060, manufacturer: 3M Co.). The calorimeter and surface temperature measurement apparatus is housed in a test section with glass walls for visual observation. The liquid is pumped from a constant temperature bath to maintain a fixed subcooling during the experiments under steady state conditions. The transient temperature data from the FFT array during flow boiling on the silicon wafer is analyzed using fast Fourier transform (FFT). The FFT data is analyzed as a function of the wall heat flux and wall superheat. The number of temperature peaks in the FFT data is observed to increase with increase in wall heat flux and the peaks are found to cover a wider spectrum with peaks at higher frequencies with enhancement of heat flux. The surface temperature fluctuations, especially at small length and time scales, are perturbed potentially by the coupled hydrodynamic and thermal transport processes, resulting in enhanced local and global heat flux values. Boiling incipience condition and the flow boiling data are compared with correlations reported in the literature.

1. Introduction

In this work we report the measurement of surface temperature fluctuations using surface micro-machined array of temperature sensors for studying micro-scale features in nucleate boiling during flow boiling conditions. This study is relevant for various thermal management applications such as spray cooling, energy conversion devices, insulation systems for cryogenic systems and energy storage, materials processing and futuristic applications (e.g. ablation cooling for high speed civil transport). An enhanced understanding of micro-scale features in flow boiling will enable the development of non-linear dynamic models for characterizing the underlying coupled hydrodynamic and thermal micro-scale mechanisms on a boiling surface.

Boiling is the most efficient mode of heat transfer. Peak heat fluxes exceeding 6 MW/m^2 have been estimated from local temperature fluctuations measured during pool boiling on horizontal surfaces (Luttich et al., 2006). These estimates were obtained by applying inverse heat conduction models on temperature fluctuation data. The temperature fluctuation data were obtained by using optical probes in the liquid pool in the vicinity of nucleating bubbles during pool boiling. However, these temperature fluctuations were reported to be sparsely distributed in space and existed for ephemeral durations (less than 2 ms).

Boiling is a highly non-linear phenomenon where the governing mechanisms for the transport processes are strongly coupled. For a given working fluid, the variables affecting boiling heat flux include wall superheat, nucleation site density, bubble diameter, contact angle, heater orientation, gravity, etc. (Dhir, 1993, 1998).

Micro-scale temperature transients during pool boiling were measured by using micro/nano-scale thermocouples (also known

* Corresponding author. Tel.: +1 979 845 4500; fax: +1 979 845 3081.
E-mail address: dbanerjee@tamu.edu (D. Banerjee).

0142-727X/$ - see front matter © 2008 Elsevier Inc. All rights reserved.
doi:10.1016/j.ijheatfluidflow.2008.08.003

Nomenclature

C_θ	constant, $C_\theta = 1 + \cos\theta$
D	diameter
h_{lv}	enthalpy of phase change (from liquid to vapor)
k	thermal conductivity
l	liquid property
ONB	onset of nucleate boiling, property value at ONB
Pr	Prandtl number
Re	Reynolds number (for liquid flow only)
sat	saturation property
T_1	temperature at thermocouple location 1
T_2	temperature at thermocouple location 2
T_w	wall temperature (or temperature on the boiling surface)
v	vapor property
w	property at wall temperature
Δx	distance between thermocouple location
ω	measurement uncertainty of an experimental parameter
θ	contact angle

as "thin film thermocouples" or "TFT") by Ahn et al. (2006). Fast Fourier transform (FFT) of the temperature fluctuations were used to estimate the temporal features. The largest value of the frequency peaks was observed to increase with wall superheat. The number of frequency peaks was also found to increase with wall superheat. These results suggest that the number of time scales for the coupled thermal and hydrodynamic features increases with increase in wall superheat. Pool boiling experiments on cylindrical heaters was used to analyze the spatially averaged experimental data for transient temperature to categorize the various regimes of boiling (Shoji, 2004; Shoji et al., 1995; Zhang and Shoji, 2003).

Significantly higher heat fluxes are associated with flow boiling than pool boiling under similar conditions of wall superheat and liquid subcooling (e.g. at boiling inception and at critical heat flux). These enhancements are primarily caused by the convective transport, acceleration/distortion of the bubble departure process as well as the resultant potential enhancement of the local surface temperature fluctuations. However, no literature data exists on the nature of local temperature transients during flow boiling on horizontal heaters.

In this study we measure the surface temperature fluctuations using temperature micro/nano-sensors fabricated on a silicon wafer during flow boiling on the silicon wafer which is heated from below. The silicon wafer is clamped on a constant heat flux type calorimeter consisting of a vertical copper cylinder with embedded cartridge heaters and K-type thermocouples. Micro/nano-thermocouples (thin film thermocouples or "TFT") are fabricated on the surface of the silicon wafer. High speed data acquisition apparatus is used to record temperature data from the TFT at 1 kHz. A fluorinert was used as the test fluid (PF-5060, manufacturer: 3M Co.).

2. Experimental setup

The experimental setup consists of the flow boiling test section, a constant temperature bath for pumping the working liquid and a high speed data acquisition unit for recording the temperatures from the experimental apparatus. The constant temperature bath consists of a digital mode chiller-heater unit (Model 9602 circulator from Polysciences Inc.). The unit consists of a cubical storage tank with a stirrer (size $26 \times 26 \times 26$ cm), a centrifugal pump which can be programmed for five different speeds ranging from 9 to 15 liters per minute, and a heat exchanger unit to digitally control the temperature of the bath. In all the experiments the Reynolds number for the working liquid was maintained at a fixed value of 4375, (based on the hydraulic diameter of the rectangular cross section of the test apparatus). The bath temperature can be regulated from −25 to 150 °C. The test section consists of a rectangular chamber housing the heater apparatus (calorimeter), along with the inlet and outlet for fluid flow. A schematic of the experimental setup is shown in Fig. 1. The test section has a 10 cm × 10 cm cross section

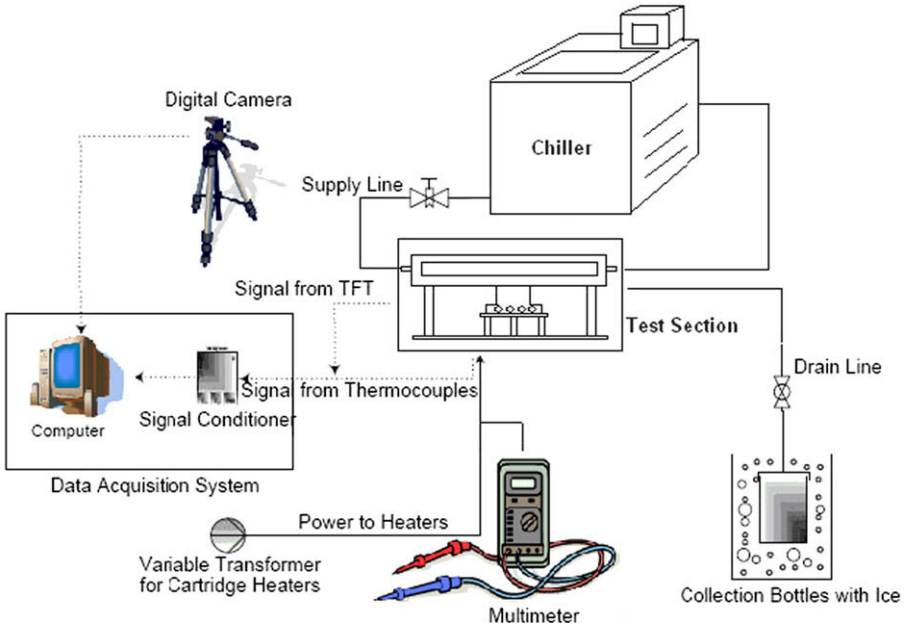

Fig. 1. Schematic layout of the experimental setup.

and is 20 cm long. The test section is made of aluminum and acetyl frames. Aluminum and Acetyl were chosen for their rigidity, low coefficient of thermal expansion and for ease of machining of the frame. The top and the two sides of the test section were fitted with glass windows visual observation of the flow boiling regime as well as to perform high speed image acquisition of the bubble formation and departure process for future flow boiling studies. The copper block was heated using 750 W cartridge heaters. Total of eight cartridge heaters were embedded into blind holes that were horizontally machined in the vicinity of the bottom edge of the copper cylinder. The cartridge heaters are used to supply 6 kW of total heat input to the copper cylinder. The power to the cartridge heater was controlled using a DC power supply (Ratings: 6.6 kW, 125 Volts, 53 A; manufacturer: Amrel Inc.). Smaller blind holes were drilled horizontally and at various radial angles into the copper cylinder at 17 locations. K-Type wire bead thermocouples were inserted in these holes to enable heat flux calculations in the vertical direction, as shown in Fig. 2. The K-type thermocouples are formed from wire bead junctions of chromel and alumel wires. K-Type thermocouple was chosen for their superior linear response (the Seebeck coefficient varies by less than ±5%) in the temperature range of interest, chemical inertness at high temperatures (both chromel and alumel alloys are doped with silicon oxide for protection against oxidation) and broad range of operating temperature (from −300 to 700 °C). Up to five pairs of thermocouples were inserted into the calorimeter to estimate the heat flux values in the vertical direction at different radial locations. These five pairs of thermocouples are separated by 5, 10.5 and 16 cm distances, as shown in the Fig. 2.

The copper cylinder is mounted on a base plate below the test section. The base plate height is adjusted to keep the test surface (mounted on the copper cylinder) to be flush with the bottom surface of the test section. For example, during the experiments with the silicon wafer the height of the base plate is adjusted so that the silicon wafer surface is flush with the bottom surface of the test section.

Additional thermocouples are placed inside the test section to monitor the liquid temperature, the temperature of the ambient and the glass windows. The surface temperature transients on

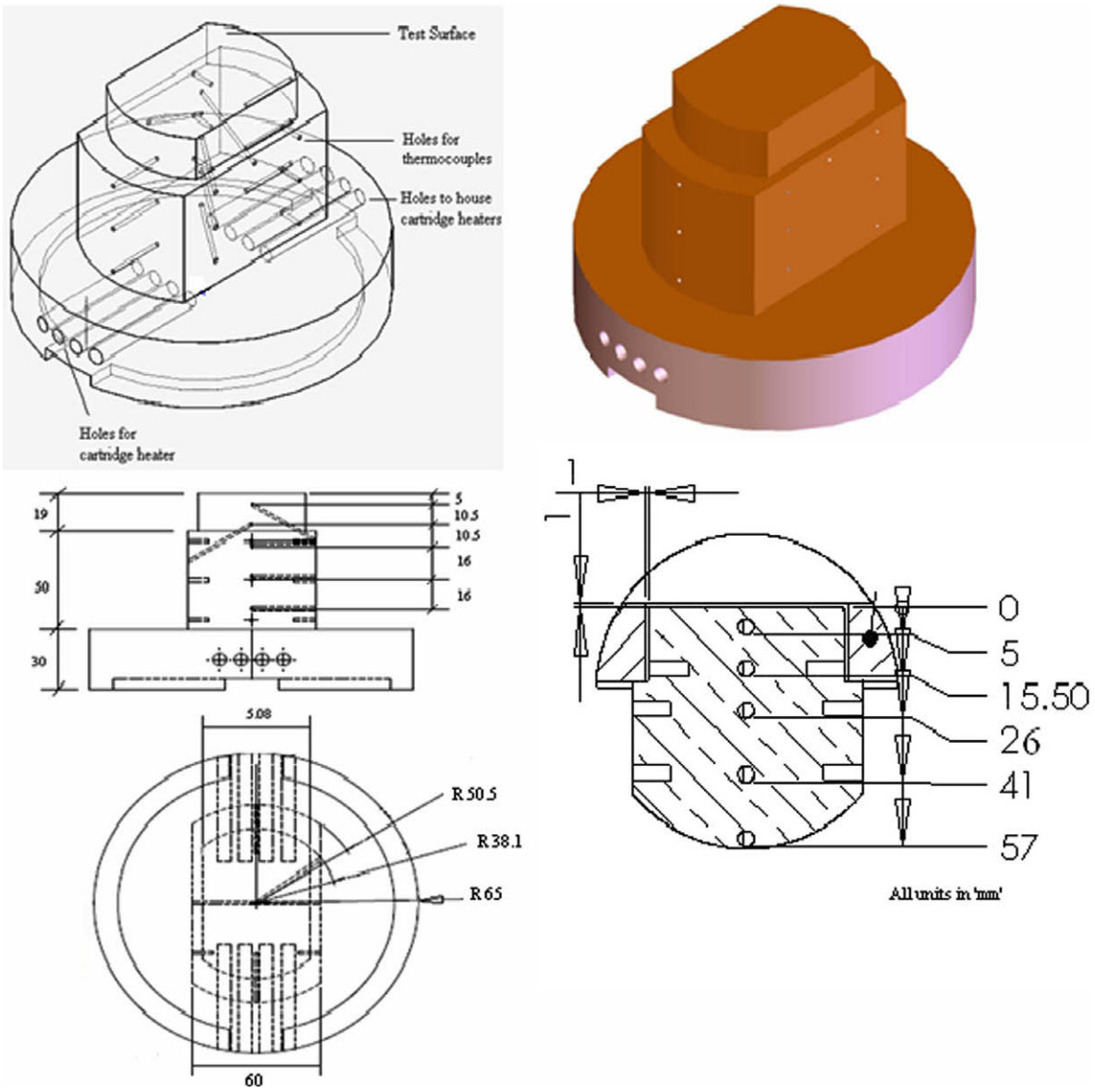

Fig. 2. Diagram showing the location of the inserted K-type thermocouples and the embedded catridge heaters in the calorimeter apparatus consisting of the machined copper cylinder.

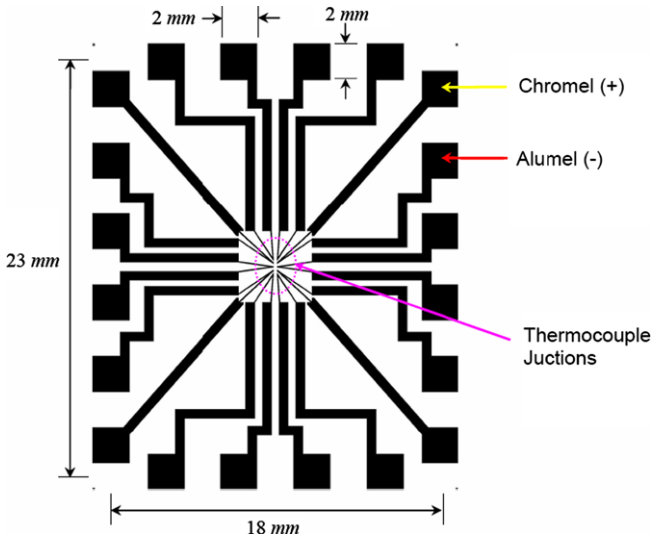

Fig. 3. Schematic showing the location of the K-type thermocouple junctions for the thin film thermocouple (TFT) array.

the silicon wafer were measured using micro/nano-sensors. The sensors consist of a thin film thermocouple (TFT) array, as shown in Fig. 3. The fabrication of the TFT array is described in the next section. All the thermocouples in the experimental apparatus are connected to a high speed data acquisition system (NI-DAQ, supplier: National Instruments). The NI-DAQ consists of an amplifier unit, a signal conditioning module, an isothermal terminal block and an *M* series multifunction device. The maximum sampling rate of the data acquisition apparatus is 100 kHz for 16 channels. Labview software (by National Instruments) was used to program and control the data acquisition unit from a desk top computer. To augment the capabilities for low noise and high bandwidth of the NI-DAQ unit, aluminum foils were used to cover the thermocouple wires and the foils were grounded to eliminate any noise captured from the ambient electro-magnetic interference (EMI) or surrounding electrical appliances in the laboratory.

3. Micro/nano-fabrication of the thin film thermocouple (TFT) array

The concept of TFT was first introduced by Marshall et al. (1966) for investigating surface temperature transients due to friction in tribological studies. The use of TFT for measuring surface temperature transients during pool boiling was first reported by Sinha (2006) and refined further by Ahn et al. (in print). A similar procedure was used for micro/nano-fabrication of the TFT array in this study. The thermocouples in this study are formed by overlapping junctions of chromel (Ni: 90% and chromium: 10%) and alumel (Ni: 95% and aluminum: 5%) patterns on a silicon wafer surface. A 3 inch diameter silicon wafer is diced in the required shape to fit the test section (Figs. 1–3). The wafer is then spin coated with a positive photoresist (SC-1827, manufacturer: MicroChem Inc.) to a thickness of 1.8 microns using a programmable spin coater. Using a photo-mask the photoresist is exposed under an ultra-violet (UV) source on a photolithography instrument (Q4000MA Mask Aligner, manufactured by Quintel). The exposed pattern on the silicon wafer is developed using MF-319 developer (manufacturer; MicroChem Inc.). The developed pattern is cleaned with DI water and an oxygen plasma "de-scum" step is performed to remove any photoresist residue in the exposed areas (this is performed to enhance adhesion of the metal layers in subsequent steps). A post exposure bake is performed to enhance mechanical rigidity and evaporate any adsorbed moisture in the unexposed photoresist layer. An adhesion layer consisting of 25 nm layer of chromium is deposited on the silicon wafer using physical vapor deposition (PVD) technique. This is immediately followed by deposition of 250 nm layer of chromel using PVD. "Lift-off" process is used to dissolve the photoresist, remove the extraneous metal thin film on the photoresist and obtain the desired metal traces (or patterns) that are deposited on the silicon wafer surface. The wafer is cleaned in an ultra sound bath using PG remover solution (manufacturer: MicroChem Inc.), to remove the photo resist. Using a different photo-mask the silicon wafer is subjected to a similar "lift-off" process to deposit chromel patterns. The junctions formed by the overlapping of the chromel and alumel patterns provide the required array of TFT. The TFT array is subsequently used in the flow boiling experiments to measure the surface temperature fluctuations on

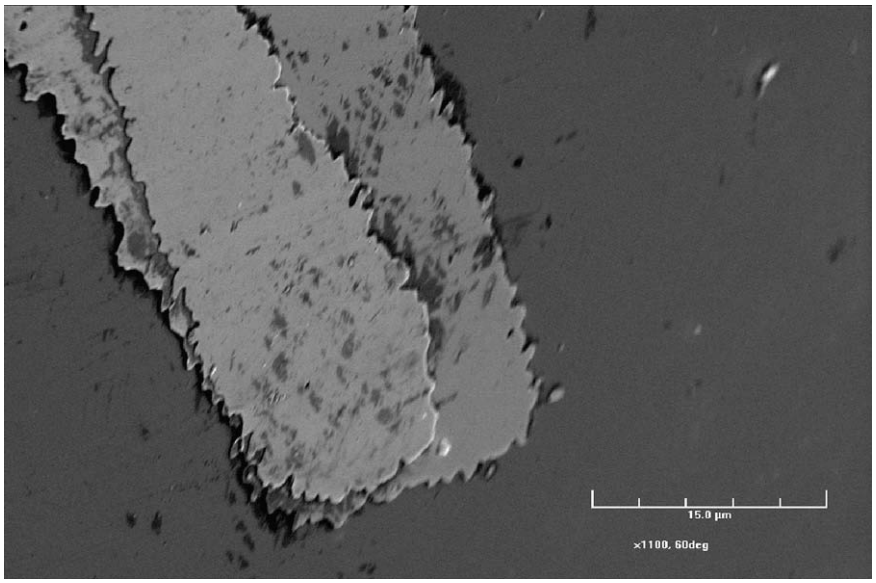

Fig. 4. Image of the K-type thermocouple junction fabricated by the overlap of the chromel and alumel thin film layers of the thin film thermocouple (TFT) array. Image was obtained by scanning electron microscopy (SEM). The TFT is 30 microns wide and 250–500 nm thick.

the silicon wafer that is heated from below. The thermocouple junctions thus formed are 30–50 microns wide and 250–500 nm in height. One of the thermocouple junctions is imaged using scanning electron microscopy (SEM) and is shown in Fig. 4. The fabricated TFTs provide high spatial and temporal resolution of the measured temperature fluctuations during the flow boiling experiments. The overall micro/nano-fabrication process for obtaining the TFT array on the silicon wafer is shown schematically in Fig. 5. At the end of the metal patterns for both chromel and alumel, square shaped "bond-pads" are incorporated as a part of the photo-mask layout design (at the opposite end of the TFT junction). The bond-pads are larger in size (larger width but same thickness) and are used to connect metal wires using wire bonding techniques for connecting to the high speed data acquisition units. Additional details about fabrication and packaging of TFT techniques, especially modified for boiling studies, are provided in Sinha (2006) and Ahn et al. (in print). The high speed data acquisition system was connected to the TFT array for acquiring temperature data at a sampling frequency of 1 kHz for each individual thermocouple in the array.

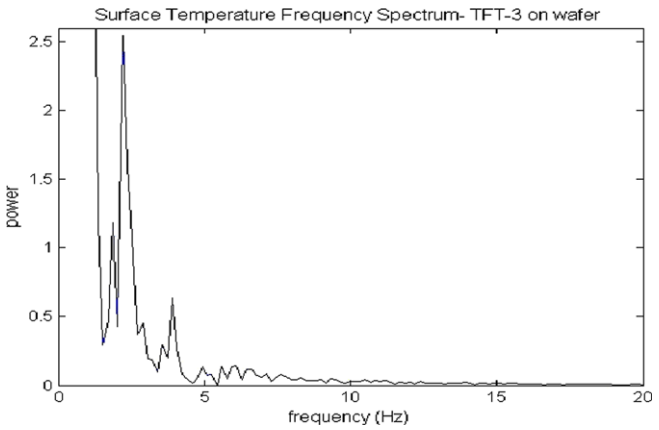

Fig. 6. Fast Fourier transform of the temperature transients obtained from a thin film thermocouple on silicon wafer at wall superheat of 7 °C and 10 °C subcooling during flow boiling at $Re = 4500$.

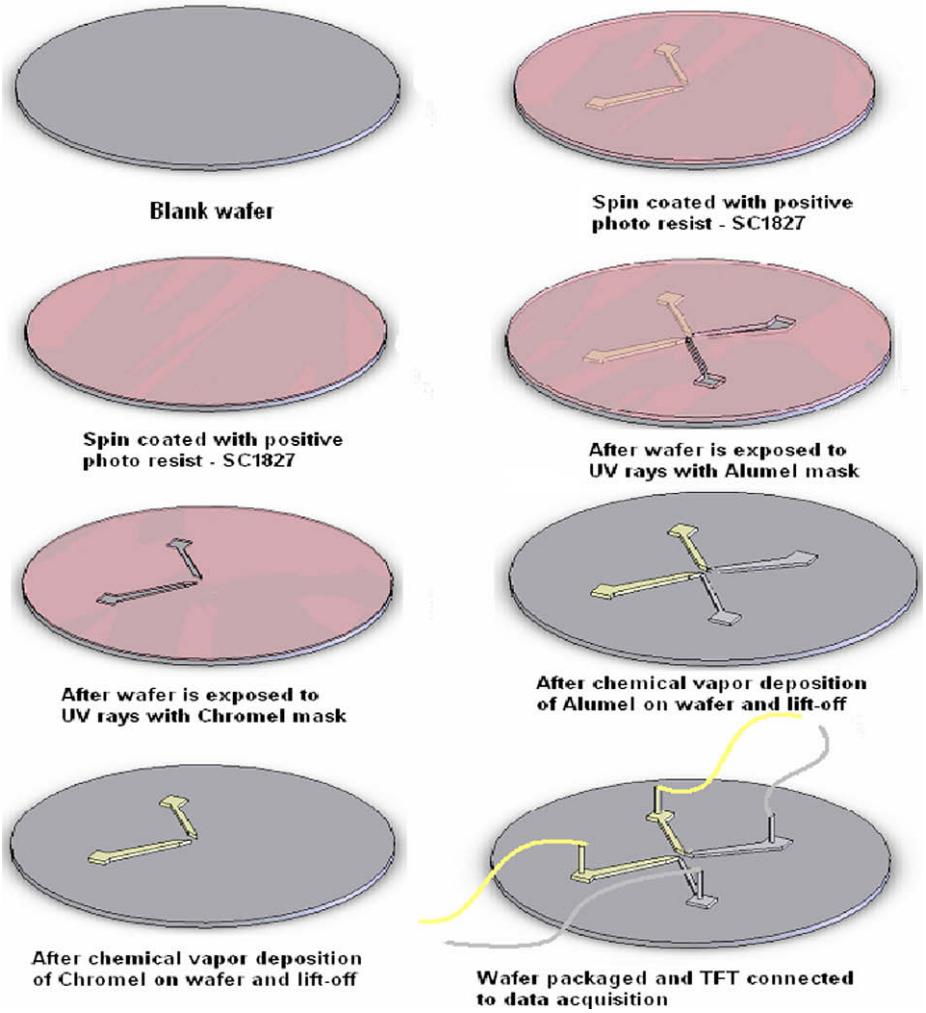

Fig. 5. Schematic showing the individual steps in the micro/nano-fabrication of thin film thermocouples (TFT) on a silicon wafer. Starting from left, top: (a) blank 3 inch diameter silicon wafer. (b) Photo resist SC-1827 is spin coated on the wafer at 3000 rpm. (c) After photolithography using photo-mask for chromel layer. (d) Patterned chromel layer after "lift-off" process (physical vapor deposition of chromel layer followed by dissolution of the underlying photoresist layer). Starting from right, top: (e) after photolithography using photo-mask for alumel layer. (f) Patterned alumel layer after "lift-off" process. (h) Wafer is packaged to form the electrical connection of the respective thermocouples layers with chromel and alumel wires.

4. Data analysis

MATLAB® software was used for analyzing the acquired transient temperature data. The collected time-temperature data were analyzed using the fast Fourier transform (FFT) technique (Brenner and Rader, 1976). FFT of the temperature fluctuations data (power versus frequency) were plotted for different wall temperatures and are as shown in Figs. 6–13. The wall heat flux data is obtained by calculating the spatial gradient of the temperature in the vertical direction at different radial locations within the copper cylinder:

$$q = k\frac{\Delta T_i}{\Delta x_i} = k\frac{T_2 - T_1}{\Delta x} \quad (1)$$

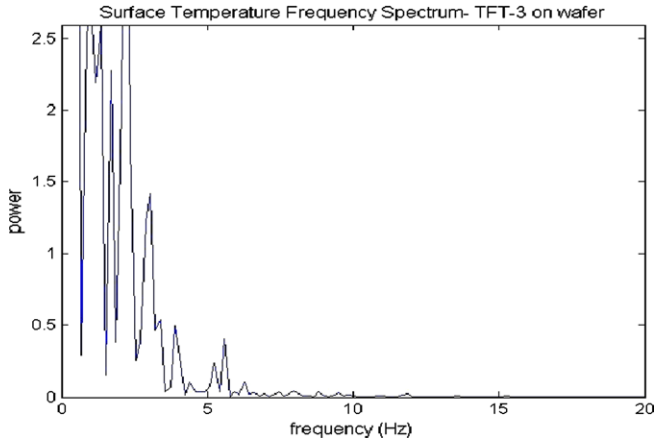

Fig. 7. Fast Fourier transform for the thin film thermocouple on wafer at 11 °C wall heat and 10 °C subcooling during flow boiling at *Re* = 4500.

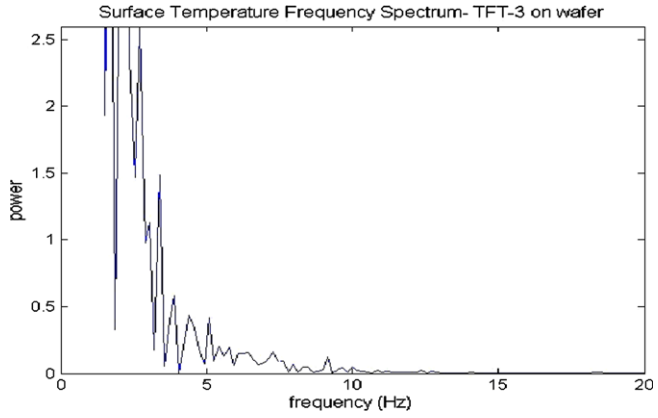

Fig. 8. Fast Fourier transform for the thin film thermocouple on wafer at wall superheat of 16 °C wall heat and 10 °C subcooling during flow boiling at *Re* = 4500.

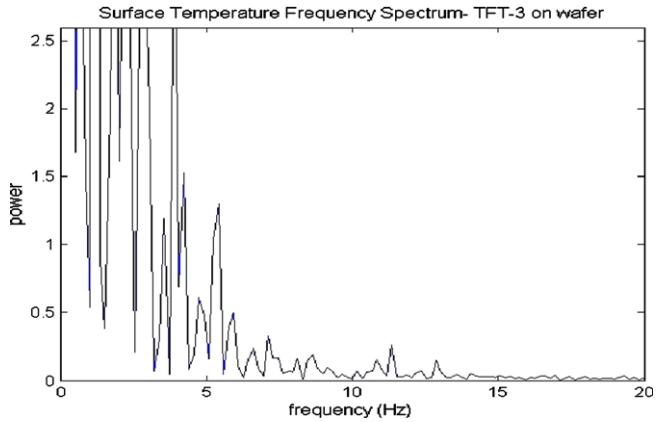

Fig. 9. Fast Fourier transform for the thin film thermocouple on wafer at 20.5 °C wall superheat and 10 °C subcooling during flow boiling at *Re* = 4500.

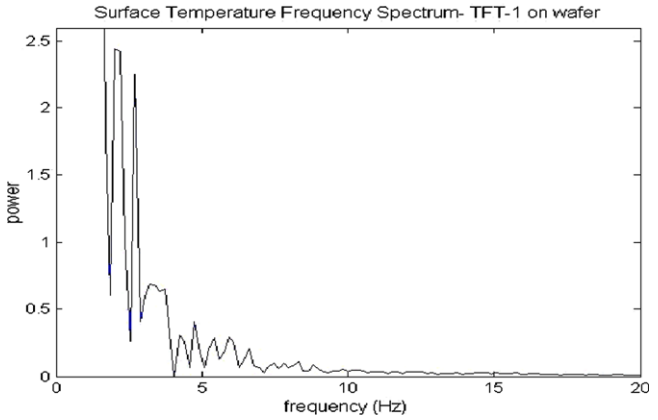

Fig. 10. Fast Fourier transform for the thin film thermocouple on wafer at 4 °C wall superheat and 14.5 °C subcooling during flow boiling at *Re* = 4500.

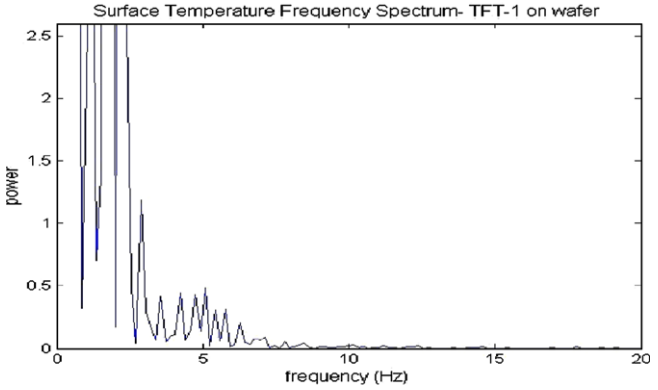

Fig. 11. Fast Fourier transform for the thin film thermocouple on wafer at 8 °C wall superheat and 14.5 °C subcooling during flow boiling at *Re* = 4500.

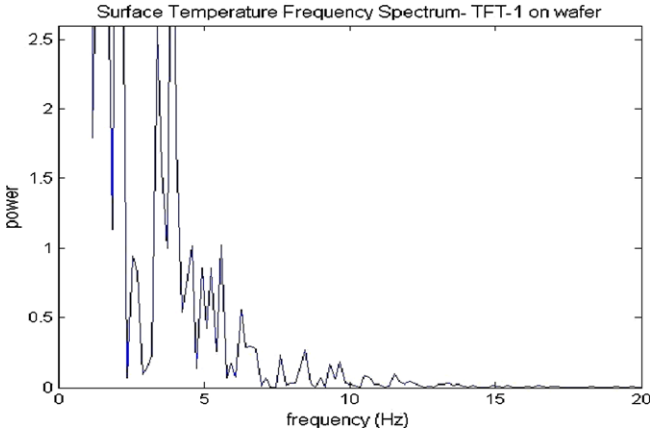

Fig. 12. Fast Fourier transform for the thin film thermocouple on wafer at 12 °C wall superheat and 14.5 °C subcooling during flow boiling at *Re* = 4500.

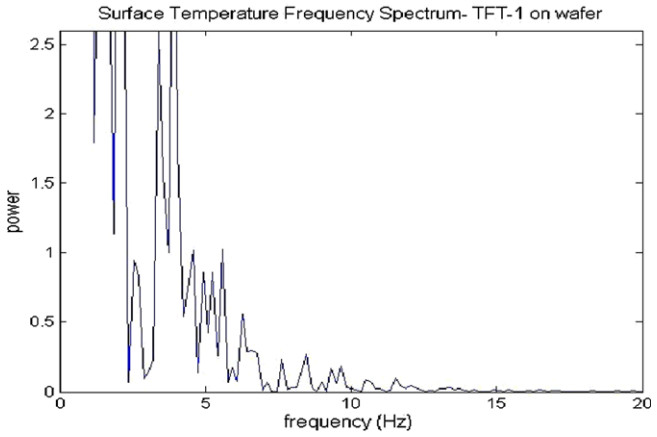

Fig. 13. Fast Fourier transform for the thin film thermocouple on wafer at 15 °C wall superheat and 14.5 °C subcooling during flow boiling at Re = 4500.

5. Experimental uncertainty

The thermocouples that are inserted into the copper block are calibrated using a NIST calibrated mercury thermometer by immersing them in a constant temperature bath (that is stirred to maintain uniform temperature). The thermocouples and TFTs are calibrated by maintaining the constant temperature bath at steady state at different temperatures. The calibration of the thermocouples is performed with a temperature stability of ±0.01 °C, which provides a measurement uncertainty of ±0.025 °C. The experimental uncertainty for estimating the heat flux in the vertical direction within the copper cylinder was estimated using the Kline and McClintock (1953) method:

$$\frac{\omega_q}{q} = \left[\left(\frac{\omega_k}{k}\right)^2 + \left(\frac{\omega_{T_1}}{T_2 - T_1}\right)^2 + \left(\frac{\omega_{T_2}}{T_2 - T_1}\right)^2 + \left(\frac{\omega_{\Delta x}}{\Delta x}\right)^2\right]^{\frac{1}{2}} \quad (2)$$

The experimental uncertainty for the wall heat flux was estimated to range from 55% at boiling inception to 23% at the maximum heat flux point.

6. Experimental results and discussion

Experiments were performed for liquid subcooling of 10 °C and 14.5 °C with the working fluid (PF-5060, manufacturer: 3M Co., saturation temperature at 1 atmosphere = 57 °C).

6.1. Surface temperature data

The wall temperature measurements were performed using TFT. The transient temperature data was analyzed using FFT techniques and are plotted in Figs. 6–13. Table 1 lists all the identified peaks which are above a threshold power of 0.1 (the noise floor was chosen to be below 0.1 based on the observation of the experimental data for FFT). It is evident from the table that the peaks and the frequency range (as well as maximum frequency) of the peaks increase with the wall temperature (T_w).

It is observed that at a given value of liquid subcooling the number of frequency peaks above the threshold power value increases with wall superheat. For example, at liquid subcooling of 10 °C, the number of peaks increases from 4 (at wall superheats of 7 °C and 11 °C) to 8 (at wall superheat of 16 °C) to 10 (at wall superheat of 20.5 °C). This increase is more dramatic at higher subcooling. At liquid subcooling of 14 °C, the number of peaks increases from 5 (at wall superheats of 4 °C) to 10 (at wall superheat of 12 °C) to 11 (at wall superheat of 15 °C).

The value of the largest frequency is observed to increase with superheat. For example, at liquid subcooling of 10 °C – the largest frequency peak increases from 6 Hz (at wall superheat of 4 °C) to 9 Hz (at wall superheat of 16 °C) to 13 Hz (at a wall superheat of 20.5 °C). This increase in highest frequency value for a given superheat is even higher for increased subcooling. For example, the largest frequency peak is at 9 Hz for wall superheat of 16 °C and liquid subcooling of 10 °C, whereas the largest frequency peak is at 12.5 Hz for wall superheat of 15 °C and liquid subcooling of 14 °C.

These phenomena can be explained by the increase in bubble nucleation density with superheat. It is expected that the bubble diameter (or volume) at departure will not change significantly with superheat since the bubble departure diameter is primarily controlled by a balance of surface tension, contact angle and buoyancy forces. Increase in bubble nucleation density can be expected to increase the spatial distribution of temperature fluctuations and the variance in the frequency of bubble departure. This implies that as the bubble nucleation density increases there is a wider distribution of the enthalpy content for each individual bubble during the bubble departure process. Thus the rate of enthalpy being carried away from the wall by the bubbles increases due to a net increase in the number (or frequency) of bubbles per unit area as well as due to a marginal increase in the variance (or the amount) of enthalpy in each departing bubble on a statistical basis.

6.2. Onset of nucleate boiling (ONB)

Onset of nucleation was observed at a wall superheat of 4 °C and 7 °C for liquid subcooling of 14.5 °C and 10 °C, respectively. The wall heat flux at onset of nucleation was measured to be 2.4 W/cm^2 and 3.3 W/cm^2 for liquid subcooling of 14.5 °C and 10 °C, respectively. Davis and Anderson (1966) proposed an elaborate correlation for predicting the wall superheat for ONB. Using this correlation the wall superheat of ONB was obtained as 0.7 °C and 0.8 °C for liquid subcooling of 10 °C and 14.5 °C, respectively. Davis and Anderson (1966) proposed the following simplified cor-

Table 1
List of frequency peaks at different wall superheats

Figure number	Wall superheat (ΔT_w, °C) $\Delta T_w = T_w - T_{sat}$	Number of peaks above 0.1 power and the frequencies	Power (magnitude) at largest frequency (Hz) (liquid subcooling, °C)
6	7	4 peaks at 5, 5.5, 6, 6.5 Hz	6.5 Hz, 0.1 power (10 °C)
7	11	4 peaks at 4, 5, 5.5, 6 Hz	5.5 Hz, 0.45 power (10 °C)
8	16	8 peaks at 4, 4.5, 5, 5.5, 5.75, 6, 7, 9 Hz	9 Hz, 0.1 power (10 °C)
9	20.5	10 peaks at 4.75, 5, 5.5, 6, 6.5, 7, 7.5, 8, 11, 13 Hz	13 Hz, 0.1 power (10 °C)
10	4	5 peaks at 4, 4.5, 5.5, 6, 6.5 Hz	6.5 Hz, 0.2 power (14 °C)
11	8	7 peaks at 3.5, 4, 4.5, 5, 5.5, 6, 6.5 Hz	6.5 Hz, 0.2 power (14 °C)
12	12	10 peaks at 4.5, 5, 5.5, 6, 6.5, 7, 7.5, 9, 9.5, 9.75 Hz	9.75 Hz, 0.2 power (14 °C)
13	15	11 peaks at 6, 6.5, 7, 7.5, 8, 9, 9.5, 10.5, 11, 11.5, 12.5 Hz	12.5 Hz, 0.45 power (14 °C)

relation for heat flux at ONB for fluids with low surface tension (e.g. at high pressures) as:

$$q_{ONB} = \frac{k_l h_{lv} \rho}{8 C_\theta \sigma T_{sat}} \left[(T_w - T_{sat})_{ONB} \right]^2 \quad (3)$$

Using this correlation at a wall superheat of 4 °C and 7 °C the heat flux value at ONB was predicted to be 2.05 W/cm^2 and 6.29 W/cm^2, respectively. Hence the observed heat fluxes were under predicted by 15% and over predicted by 88% by this correlation.

This correlation (Eq. (3)) is similar to that proposed by Sato and Matsumara (1964). However, the latter correlation does not account for contact angle. Using Sato and Matsumara (1964) correlation the heat flux value would be 98% higher than the values predicted by the Davis and Anderson (1966) correlation, since the contact angle for the test fluid (PF-5060) is ~10° on silicon.

To account for property variations for different fluids, Frost and Dazlowic (1967) modified Eq. (3) and proposed the following correlation:

$$q_{ONB} = \frac{k_l h_{lv} \rho}{8 \sigma T_{sat}} \left[(T_w - T_{sat})_{ONB} \right]^2 Pr_v^2 \quad (4)$$

Using this correlation at a wall superheat of 4 °C and 7 °C the heat flux value at ONB was predicted to be 2.68 W/cm^2 and 8.19 W/cm^2, respectively. Hence the observed heat fluxes were over predicted by 10% and 145% by this correlation, respectively.

These predictions therefore under predicted the wall superheat required for the ONB condition while over predicting the heat flux observed at the ONB condition. This is to be expected since the correlations were obtained for commercially prepared surfaces which have a propensity for higher nucleation density of bubbles compared to the silicon wafer surface employed in this study. The silicon wafer surface is atomically smooth (a single crystal plane is exposed in these wafers). Therefore, it is expected that the nucleation site density will be orders of magnitude less than the surfaces used in the correlation. Also, this would explain the higher wall superheat required for ONB than predicted by the correlations since commercially prepared surfaces have a wider distribution of cavities which cause ONB to occur at a lower superheat for larger cavities. In this study the atomically smooth silicon wafer does not have any cavities for nucleation to occur. Consequently, higher wall superheats are required for nucleation incipience on the silicon wafers. Nucleation was observed to initiate on the edges as well as the bond pads and the wire connectors on the periphery of the silicon wafer (that were used for connecting the TFT array on the surface). Following the nucleation at the edges and at the periphery – additional nucleation was observed on the whole wafer surface at higher wall superheats.

6.3. Heat flux data

The heat flux in the copper block in the vertical direction was calculated at different wall temperatures using Eq. (1). The heat flux data is listed in Table 2, corresponding to liquid subcooling of 10 °C and 14.5 °C. Table 2 shows that the pool boiling heat flux increases with superheat and subcooling, as would be expected.

Rosenhow (1953) proposed that the total heat flux in flow boiling is composed of two components: that due to single phase liquid convection (q_{spl}) and that due to nucleate boiling (q_{nb}). It was proposed that the single phase component can be calculated using a conventional estimate for single phase internal flow heat transfer coefficient, e.g., Dittus and Boelter (1930) correlation (Incropera and Dewitt, 1996). The additional nucleate boiling contribution to the total heat flux can be calculated using the Rosenhow (1952) correlation. The heat flux data obtained in this study was compared to the predictions from the Rosenhow (1953) model and is plotted in Figs. 14 and 15. It is observed that the predictions from the correlations match the experimental data for liquid subcooling of 14.5 °C within the limits of the experimental uncertainty (except at the ONB). At liquid subcooling of 14.5 °C the correlation over predicts the heat flux data by 9% at low wall superheats (except at the ONB) and under predicts the heat flux data by 12% at higher wall superheats. Similarly at liquid subcooling of 10 °C the correlation over predicts the heat flux data by 26% at low wall superheats (except at the ONB) and over predicts the heat flux data by 4% at higher wall superheats. Hence the Rosenhow (1953) model is found to be in good agreement with the observed experimental data (except at the ONB).

Table 2
Wall heat flux data for different wall superheats and liquid subcooling during flow boiling at Re = 4375

Wall superheat (ΔT_w, °C) $\Delta T_w = T_w - T_{sat}$	Heat flux (q, W/cm^2)	Liquid subcooling (Re = 4375)
7	3.34	10 °C
11	6.35	10 °C
16	10.26	10 °C
20.5	14.32	10 °C
4	2.43	14.5 °C
8	5.39	14.5 °C
12	8.40	14.5 °C
15	11.76	14.5 °C
17.5	14.5	14.5 °C

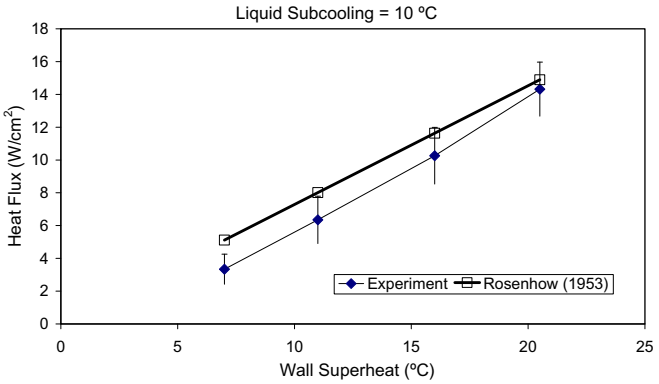

Fig. 14. Comparison of flow boiling heat flux data with Rosenhow (1953) model for liquid subcooling of 10 °C.

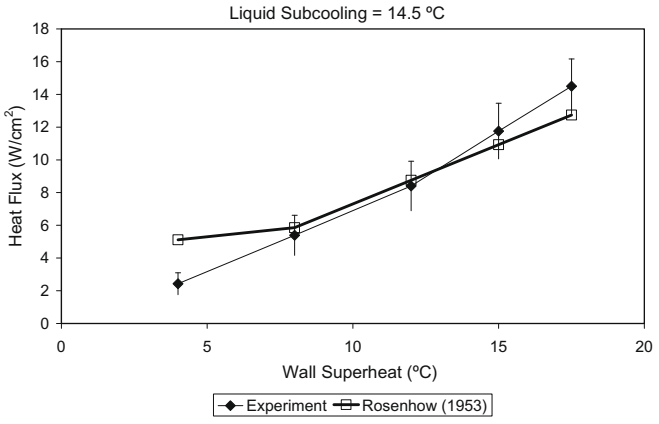

Fig. 15. Comparison of flow boiling heat flux data with Rosenhow (1953) model for liquid subcooling of 14.5 °C.

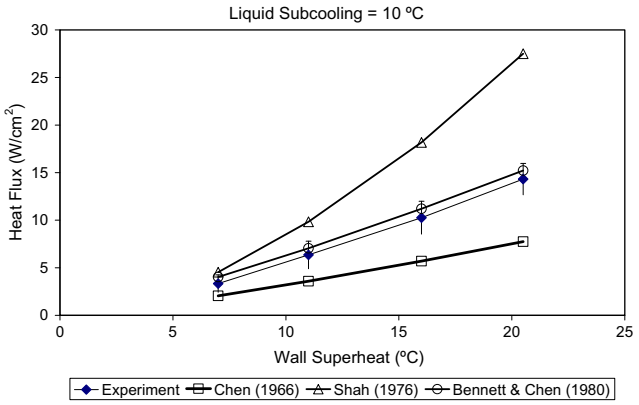

Fig. 16. Comparison of flow boiling heat flux data with Chen (1966) model, Bennett and Chen (1980) model and Shah (1976) model for liquid subcooling of 10 °C.

Additional comparisons were made with forced convective boiling models proposed by Chen (1966) and Shah (1976). Figs. 16 and 17 show the comparison of experimental data with these predictions. It is observed that at liquid subcooling of 10 °C the Chen correlation under predicts the heat flux data by 39% at low wall superheats and under predicts the heat flux data by 46% at higher wall superheats. At liquid subcooling of 14.5 °C the Chen correlation under predicts the heat flux data by 52–58% for all values of wall superheats. At liquid subcooling of 10 °C the Shah correlation over predicts the heat flux data by 36% at low wall superheats and over predicts the heat flux data by 92% at higher wall superheats. At liquid subcooling of 14.5 °C the Shah correlation over predicts the heat flux data by 22% at low wall superheats (except for ONB condition where it underpredicts by 9%) and over predicts the heat flux data by 47–63% at higher wall superheats. The Shah correlation is reported to have an error of 30% over the experimental data used to generate the correlations.

Bennett and Chen (1980) proposed an improvement to their earlier model by accounting for the property variation in their model for different fluid properties. They proposed that the heat flux data be multiplied by a correction factor (equal to $Pr_l^{0.296}$). After adjusting for this correction factor, the values obtained from this model are plotted in Figs. 16 and 17. At liquid subcooling of 10 °C the Bennett and Chen (1980) correlation under predicts the heat flux data by 10–20% at low wall superheats and over predicts the heat flux data by 6–11% at higher wall superheats. At liquid subcooling of 14.5 °C the Bennett and Chen (1980) correlation under predicts the heat flux data by 11–17% at low wall superheats and over predicts the heat flux data by 7–14% at higher wall superheats. These predictions match the experimental data very well within the limits of the experimental uncertainty.

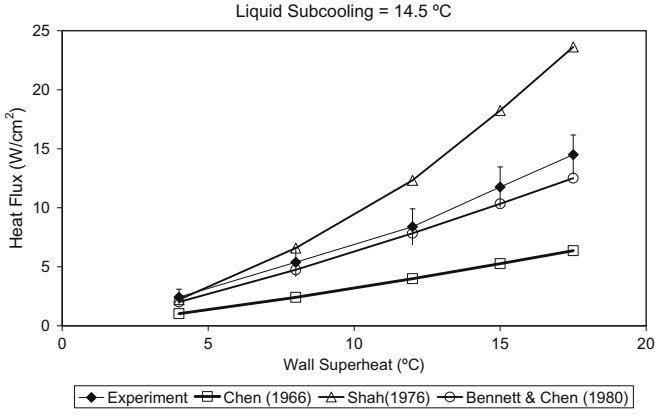

Fig. 17. Comparison of flow boiling heat flux data with Chen (1966) model, Bennett and Chen (1980) model and Shah (1976) model for liquid subcooling of 14.5 °C.

The comparison with the correlation in the literature shows that the Rosenhow (1953) model as well as Bennett and Chen (1980) model provide the best match for the experimental data. The experimental data is under predicted by the Chen correlation and over predicted by the Shah correlation. A potential reason for the good match with Rosenhow's model is because this model is based on a physical model. This physical model is based on dividing the heat flux into two components which are assumed to vary fairly independent of each other (single phase liquid convection and nucleate boiling). In general, in the fully developed nucleate boiling and at critical heat flux (CHF) the boiling process is fairly independent of the convection mediated transport processes – since lateral/vertical merger of nucleating bubbles at the wall – are the dominant mechanisms for heat transfer rather than the bubble departure process itself (which is the dominant transport mode at onset of nucleate boiling).

In contrast the Shah correlation and Chen correlation are based on heuristic approaches where the correlations are obtained by regression analyses of experimental data based on several non-dimensional parameters (e.g. boiling number and liquid flow only Froude numbers). These models are based on the assumption that the two phase heat flux is a multiple of the single phase heat transfer. The multiplying factor is estimated using heuristic approaches (or behavioral models rather than physical models). Hence, it is expected that these correlation will deviate from experimental data when the conditions are distinctly different from the original experiments the correlations are based on. In the present study, an atomically smooth wafer silicon wafer was used which is expected to have a different nucleation density distribution at different superheats compared to experiments based on commercial surfaces. Also, a refrigerant is used (instead of water – which is typically used as the test fluid in the Chen model and the Shah model). Hence, when the fluid property variations are accounted for (as in the Bennett and Chen model) – the experimental data are found to match the predictions very well and both predictions are found to be within the bounds of the experimental uncertainty.

At the ONB, the single phase transport processes can affect the boiling incipience conditions (and vice versa). Therefore the two components of the total heat flux are not independent of each other. Rosenhow's model violates this condition and therefore does not match the ONB heat flux data. In contrast, the heuristic models proposed by Chen (1966), Shah (1976) as well as Bennett and Chen (1980) match the ONB data very well. This potentially shows that the ONB condition is governed by highly complex coupled and non-linear processes that are better described using statistical models (e.g. regression analyses) rather than by physical models (e.g. mechanistic models; Dhir, 1998) or behavioral models (e.g. chaos theory or fractal models; Shoji, 2004).

7. Conclusion

The results from the FFT analyses show that the number of frequency peaks increases as the wall superheat increases. This enhancement is even more pronounced at higher subcooling. This result implies that there is an increase in the diversity of the spatio-temporal scales for the different coupled thermal and hydrodynamic transport mechanisms with increase in superheat and subcooling. Closer analysis of the FFT graph shows that above a threshold power level of 0.1, the maximum value of the peaks in frequency domain increases to higher values with increase in both superheat and subcooling. This can be explained to be due to increase in bubble nucleation density with superheat, as well as

due to higher enthalpy content of each bubble with increase in superheat and subcooling.

The onset of nucleate boiling (ONB) is found to occur at higher wall superheats and yields lower values of heat flux compared to the values obtained from correlations reported in the literature. The results show that the ONB condition is better described by statistical models than by physical or behavioral models.

The flow boiling curve (wall heat flux as a function of wall superheat) is found to match the flow boiling model proposed by Rosenhow (1953) as well as by the Bennett and Chen (1980) model. The models proposed by Shah (1976) over predicts the heat flux data while the model proposed by Chen (1966) is found to under predict the heat flux data. The correlations that account for the transport processes (Rosenhow) and fluid property variations (Bennett and Chen) are found to be in good match with experimental data.

Acknowledgements

This work was supported by the United States Office of Naval Research. The authors thank Mr. I. Ramirez for his help with the assembly of the experimental apparatus.

References

Ahn, H.S., Vijaykumar, S., Banerjee, D., Lau, S., 2006a. Pool boiling experiments on multi walled carbon nanotubes and using surface-micromachined temperature sensors. In: Proceedings of the AIAA/ASME Joint Thermophysics Conference, San Francisco, CA, June 3–8.

Ahn, H.S., Sinha, N., Zhang, M., Feng, S., Banerjee, D., Baughman, R., 2006b. Pool boiling experiments on multi walled carbon nanotube (MWCNT) forests. ASME Journal of Heat Transfer 128 (12), 1335–1342.

Ahn, H.S., Sinha, N., Williams, R., Banerjee, D., in print. Packaging of surface-micromachined thin film thermocouples (TFT): Comparison of the resistance arc micro-welding technique with wire bonding. IEEE Transactions in Components and Packaging Technology.

Bennett, D.L., Chen, J.C., 1980. Forced convective boiling in vertical tubes for saturated pure components and binary mixtures. AICHE Journal 26, 66–86.

Brenner, N., Rader, C., 1976. A new principle for fast Fourier transformation. IEEE Journal of Acoustics, Speech & Signal Processing 24, 264–266.

Chen, J.C., 1966. Correlation for boiling heat transfer to saturated fluid in convective flow. Ind. Chem. Proc. Design and Dev. 52 (No. 3), 322–339.

Davis, E.J., Anderson, G.H., 1966. The incipience of nucleate boiling in forced convection flow. AICHE Journal 12, 774–780.

Dhir, V.K., 1993. Heat Transfer. McGraw-Hill Encyclopedia of Science and Technology, 169–171.

Dhir, V.K., 1998. Boiling heat transfer. Annual Review of Fluid Mechanics 30, 365–401.

Dittus, F.W., Boelter, L.M.K., 1930. Publications on Engineering, vol. 2. University of California Berkeley Press. pp. 443.

Frost, W., Dazlowic, G.S., 1967. An extension of the methods of predicting incipient boiling on commercially finished surfaces. ASME Paper No. 67-HT-61, 1967 National Heat Transfer Conference, Seattle, WA.

Incropera, F.P., Dewitt, D.P., 1996. Fundamentals of Heat and Mass Transfer, fourth ed. Wiley Publications. pp. 445.

Kline, S.J., McClintock, F.A., 1953. Describing uncertainties in single sample experiments. Mechanical Engineering 75 (1), 38.

Luttich, T., Marquardt, W., Buchholz, M., Auracher, H., 2006. Identification of unifying heat transfer mechanisms along the entire boiling curve. International Journal of Thermal Sciences 45, 284–298.

Marshall, R., Atlas, L., Putner, T., 1966. The preparation and performance of thin film thermocouples. Journal of Scientific Instruments 43, 144–149.

Rosenhow, W.M., 1952. A method of correlating heat transfer data for surface boiling of liquids. Transactions of the ASME 84, 1969.

Rosenhow, W.M., 1953. Heat transfer with evaporation. In: Proceedings of the Heat Transfer Symposium, University of Michigan Ann Arbor, pp. 101–150.

Sato, T., Matsumara, H., 1964. Bulletin of the Japan Society of Mechanical Engineers 7, 392.

Shah, M.M., 1976. A new correlation for heat transfer during boiling flow through pipes. ASHRAE Transactions 82 (Part 2), 66–86.

Shoji, M., Kohno, T., Negishi, J., Toyoshima, S., Maeda, A., 1995. Chaos in boiling on a small-size heater. In: Proceedings of the Fourth ASME-JSME Thermal Engineering Joint conference, Maui, vol. 2, pp. 225–232.

Shoji, M., 2004. Studies of boiling chaos: a review. International Journal of Heat and Mass Transfer 47, 1105–1128.

Sinha, N., 2006. Design, fabrication, packaging and testing of thin film thermocouples for boiling studies. M.S. Thesis, Texas A&M University.

Zhang, L., Shoji, M., 2003. Nucleation site interaction in pool boiling on the artificial surface. International Journal of Heat and Mass Transfer 46, 513–522.